Extending the Applicability Range of Compressive Sensing-Based Microwave Imaging to Arbitrary Scatterers

N. Alselmi, G. Oliveri, M. A. Hannan, M. Salucci, and A. Massa

Abstract

This work deals with an innovative two-dimensional (*2D*) free-space microwave imaging technique. The developed inverse scattering (*IS*) technique is aimed at enabling Compressive Sensing (*CS*) to deal with the retrieval of unknown scatterers which are not necessarily sparse in the standard sense, i.e., in the pixel domain. Accordingly, the proposed technique exploits a user-defined *dictionary* of expansion bases that are used to retrieve several guesses of the electromagnetic properties of the investigation domain. Then, following the *BCS* paradigm, the *sparsest* solution is recognized as the optimal one. Some numerical results are presented, in order to verify the effectiveness of the proposed *IS* technique for imaging scatterers with arbitrary size and shape.

1 Numerical Results

1.1 Object Haar #1

Goal: To prove the effectiveness of the alphabet based approach using an "ad-hoc" scatterer for Haar wavelets.

Test Case Description

Object:

- $\varepsilon_{r,max} = 1.04$
- $\sigma = 0$ [S/m]
- Number of Haar coefficients: $Nc = 21$

Sources:

- Plane waves
- Amplitude: $A = 1$
- Frequency: 300 MHz ($\lambda = 1$m)
- Number of views: $V = 36$

Direct solver:

- Square domain divided in $\sqrt{D} \times \sqrt{D}$ cells
- $D = 4096$ (64×64) $(\frac{L_D}{\sqrt{D}} = \frac{\lambda}{16})$

Investigation domain:

- Square domain divided in $\sqrt{N} \times \sqrt{N}$ cells
- $N = 1024$ (32×32) $(\frac{L_D}{\sqrt{N}} = \frac{\lambda}{8})$
- $L_D = 4\lambda$

Measurement domain:

- Measurement points taken on a circle of radius $\rho = 4\lambda$
- $M = 36$

M-BCS parameters:

- $a = 1.0 \times 10^{-2}$
- $b = 1.0 \times 10^{-5}$

RESULTS - Best Retrieved Object

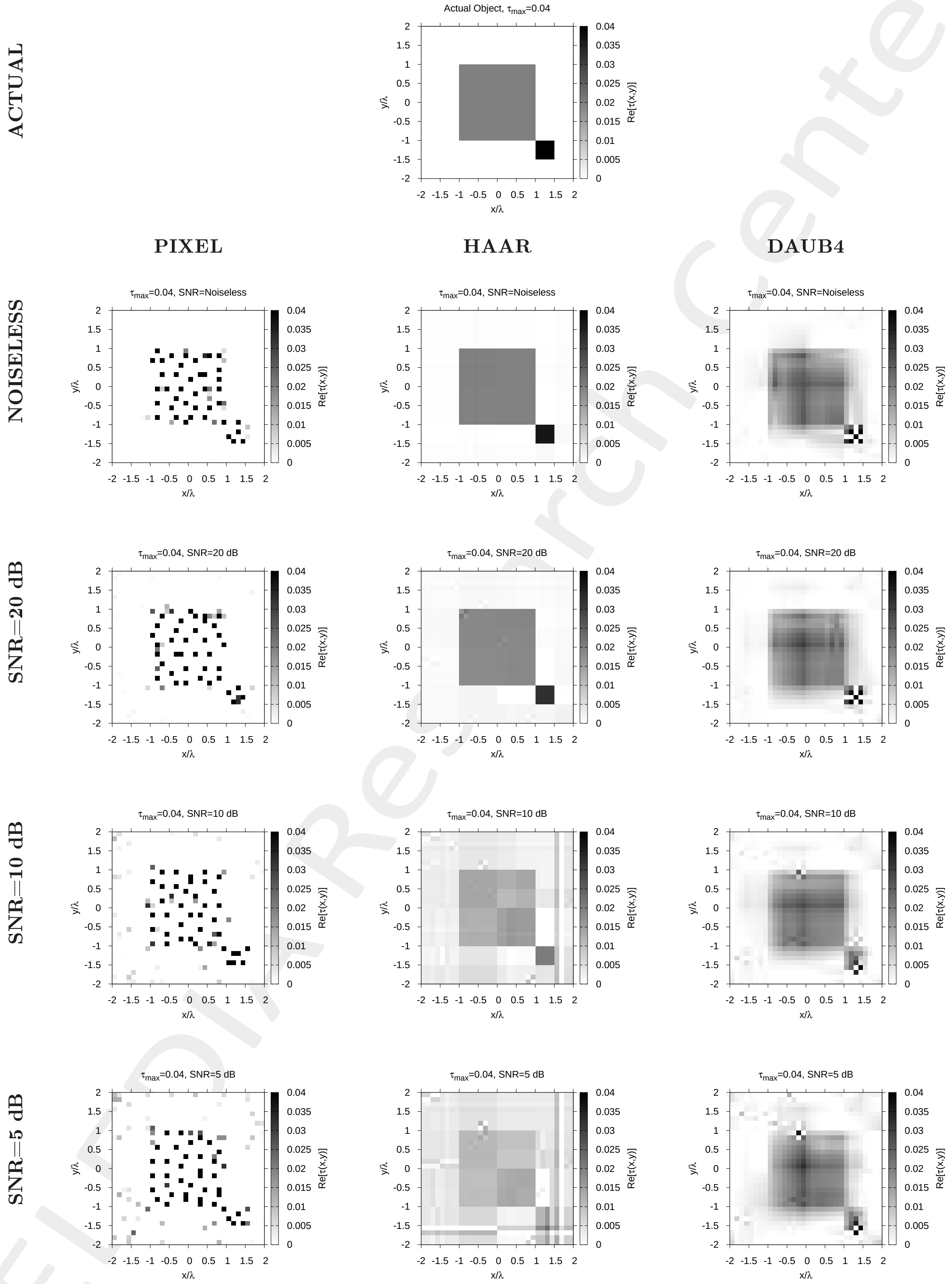

Figure 1: Actual and retrieved object (real part) considering different wavelet expansions.

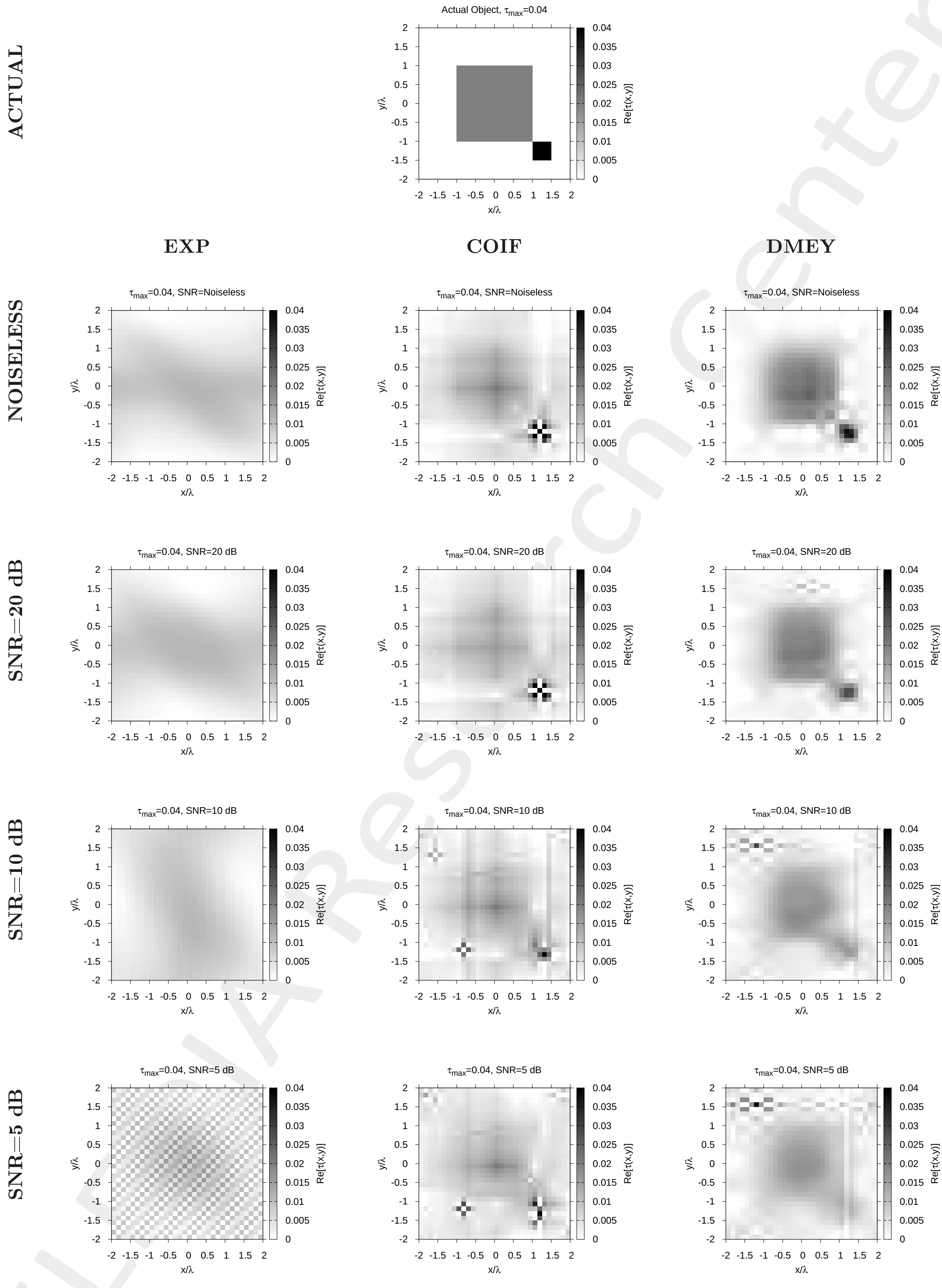

Figure 2: Actual and retrieved object (real part) considering different wavelet expansions.

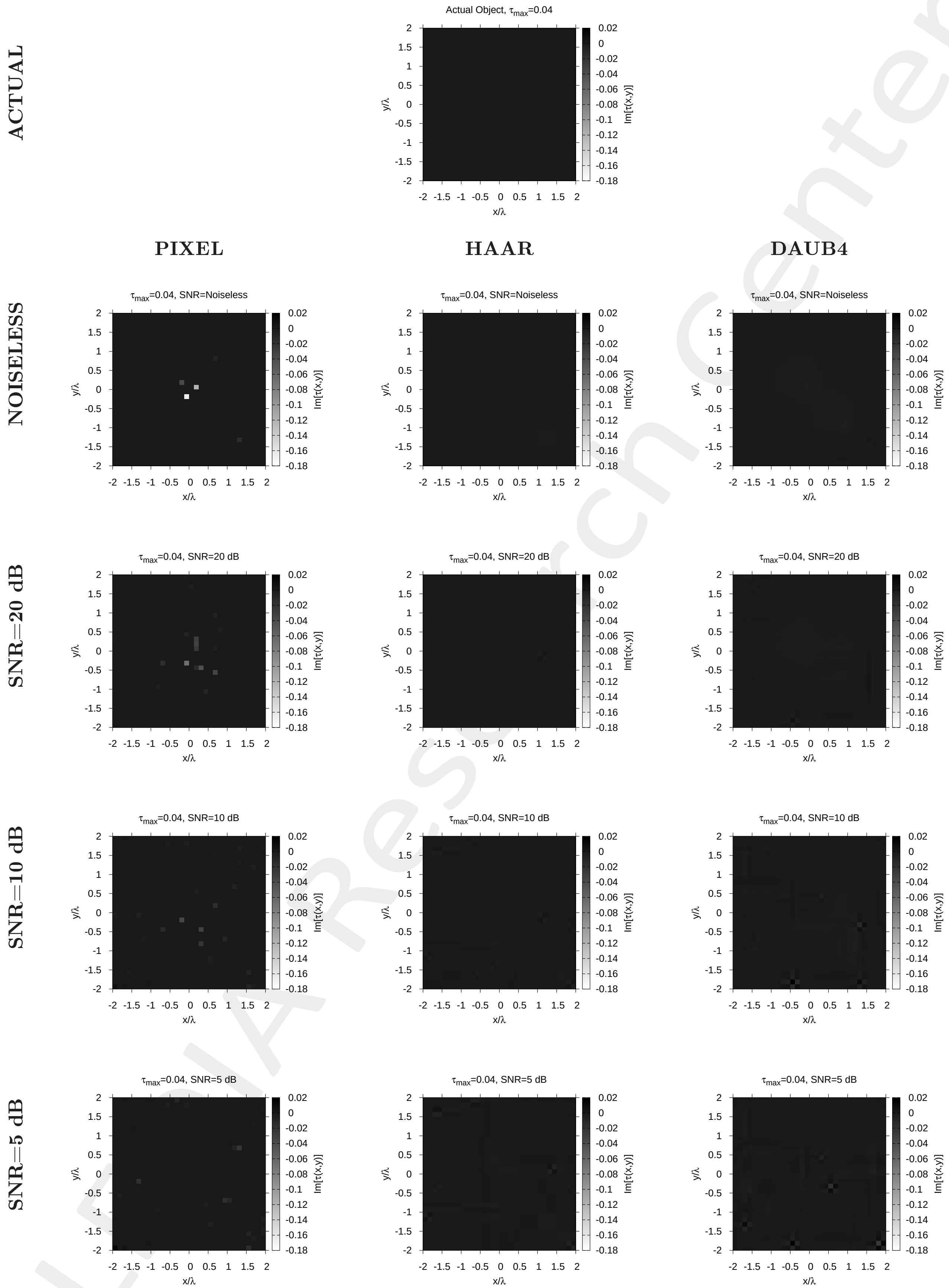

Figure 3: Actual and retrieved object (imaginary part) considering different wavelet expansions.

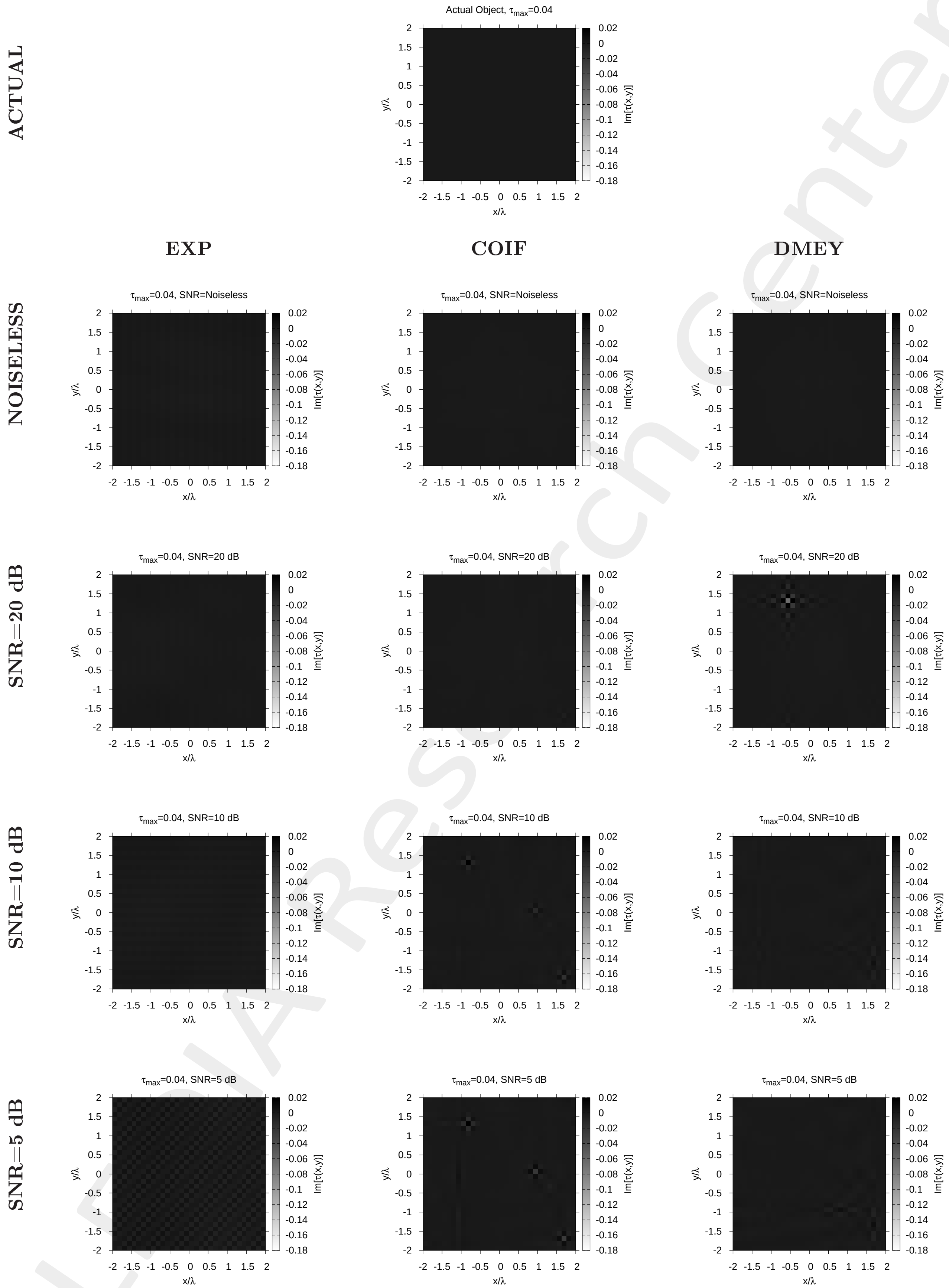

Figure 4: Actual and retrieved object (imaginary part) considering different wavelet expansions.

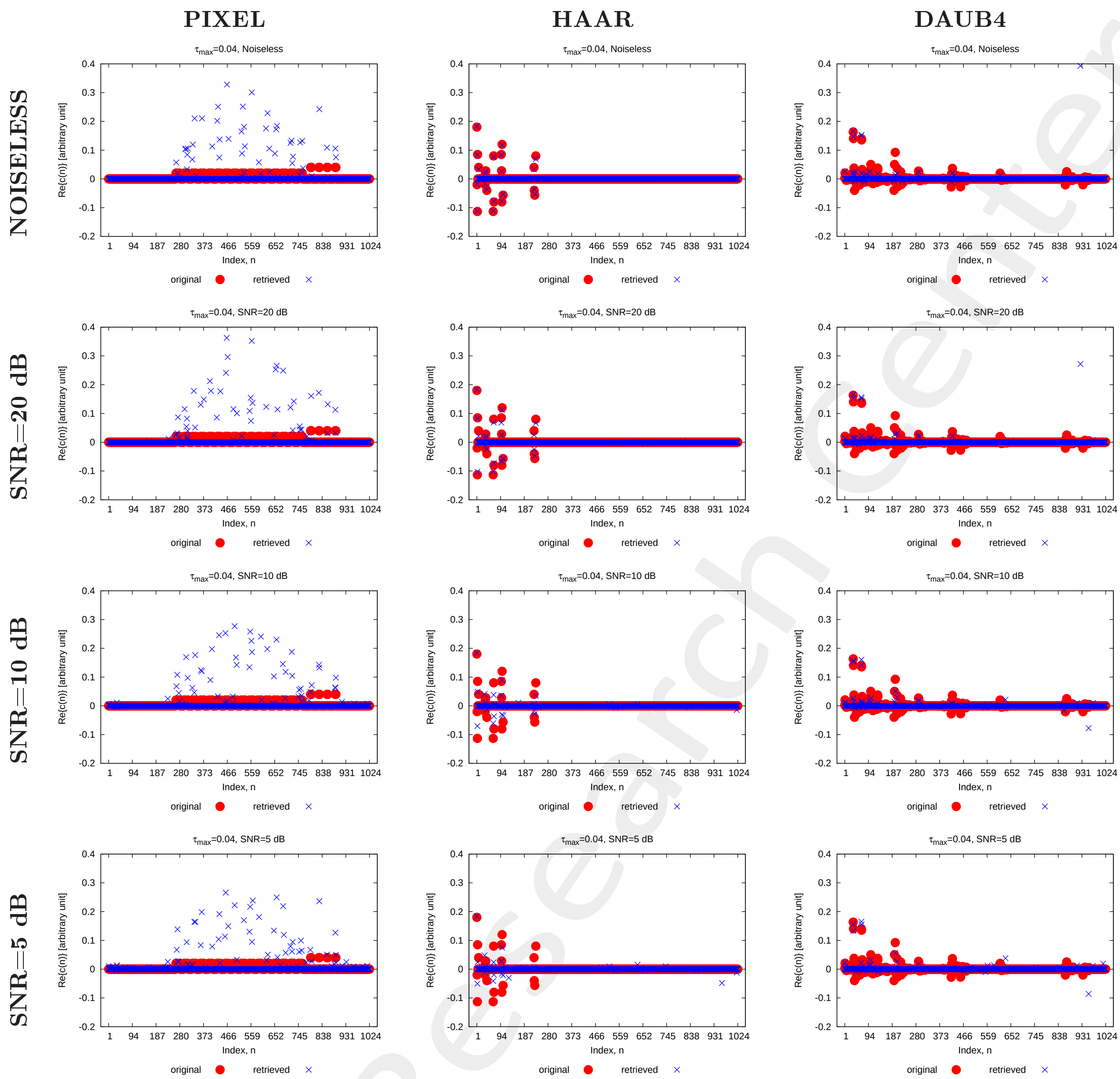

Figure 5: Real part of the actual and retrieved coefficients considering different wavelet expansions.

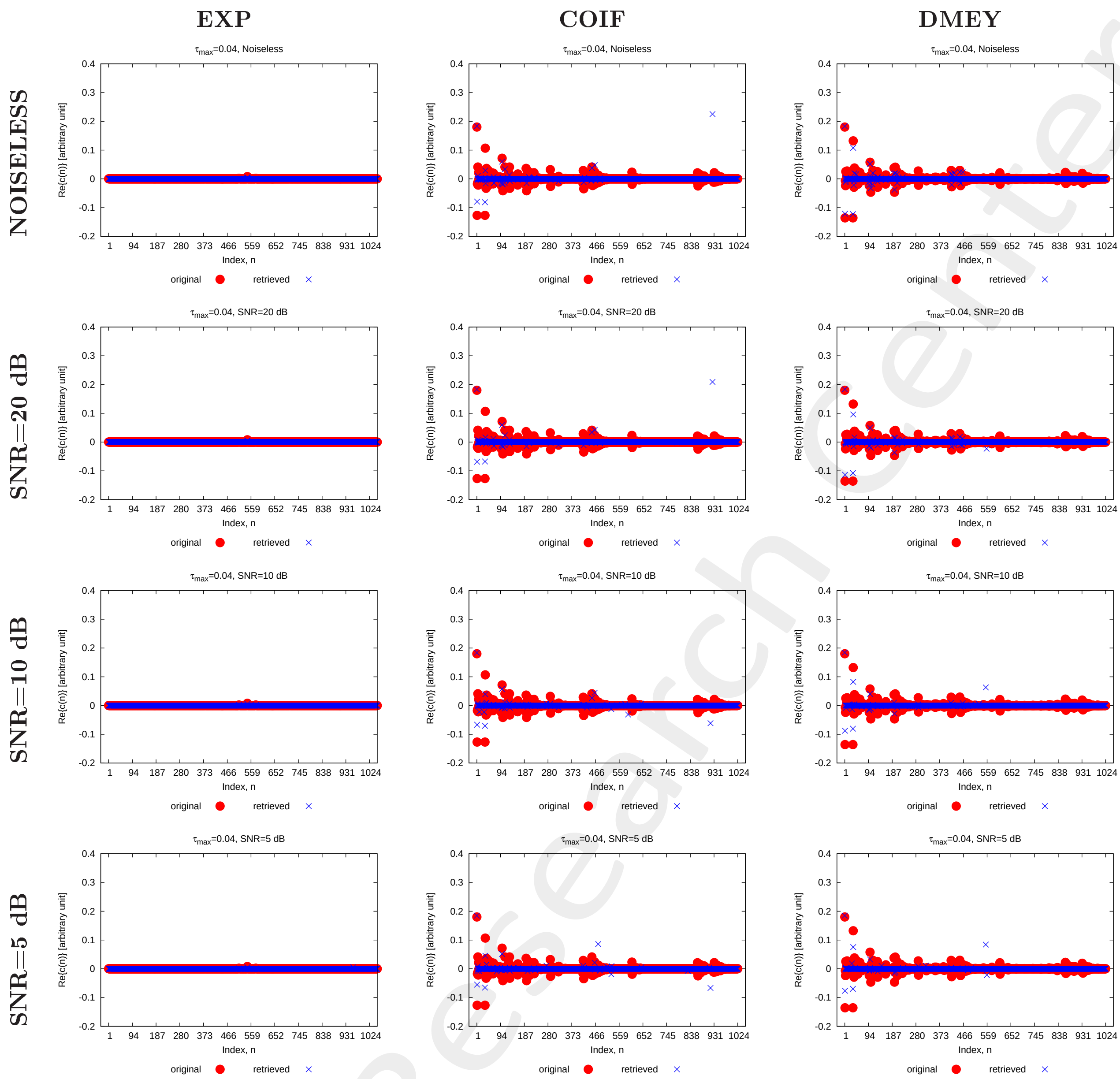

Figure 6: Real part of the actual and retrieved coefficients considering different wavelet expansions.

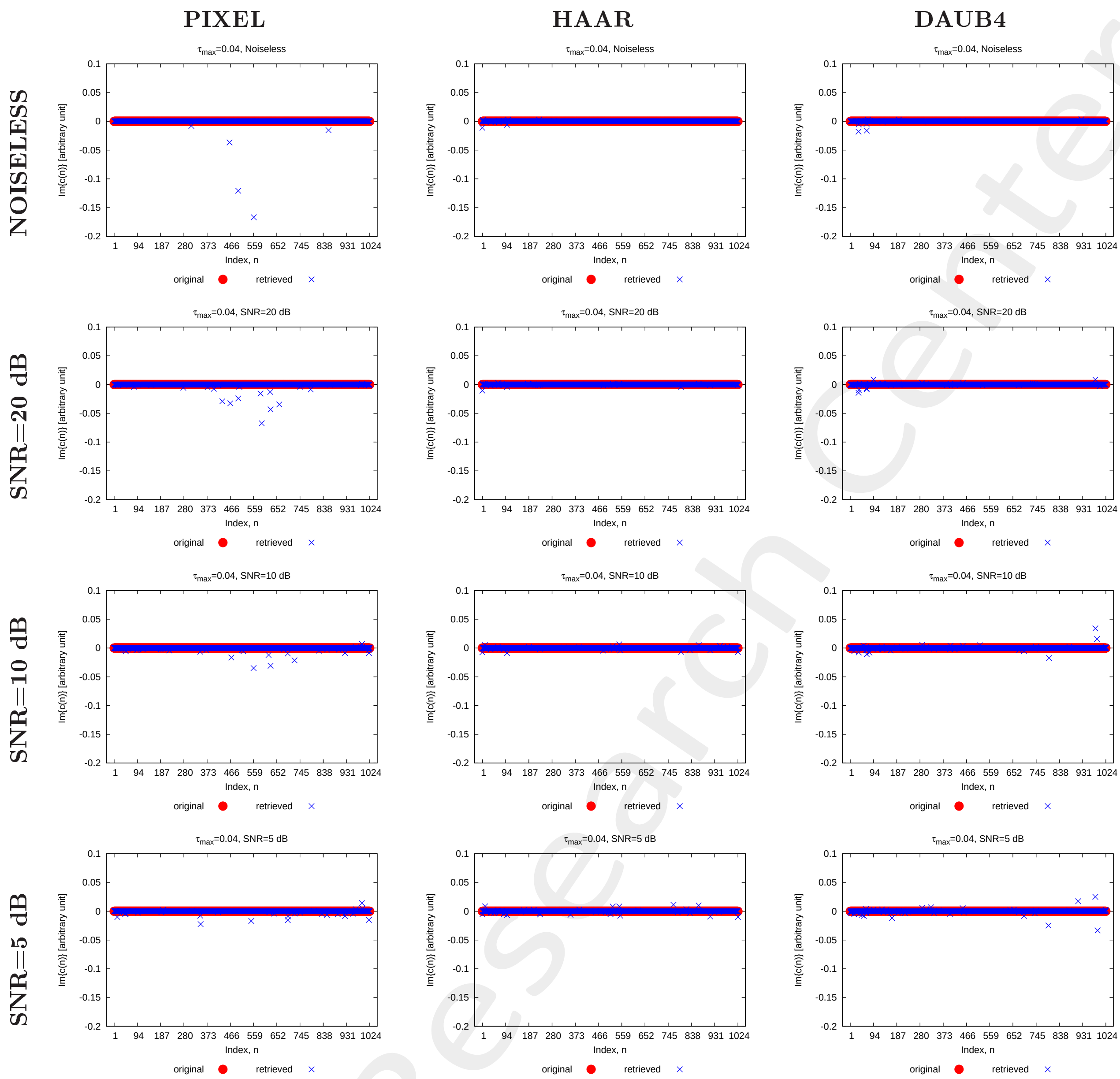

Figure 7: Imaginary part of the actual and retrieved coefficients considering different wavelet expansions.

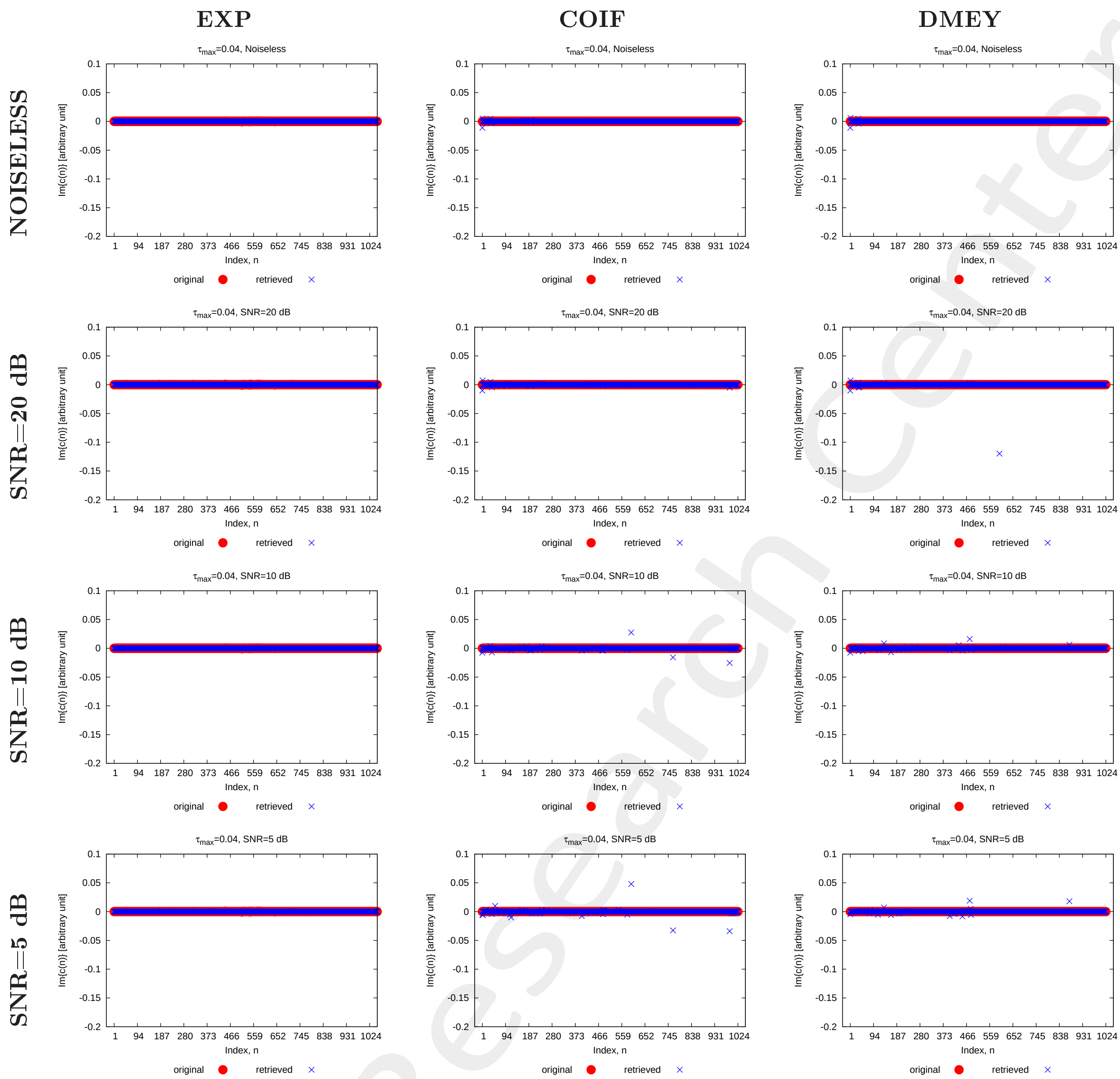

Figure 8: Imaginary part of the actual and retrieved coefficients considering different wavelet expansions.

Coefficients Analysis $T = 100\%$:

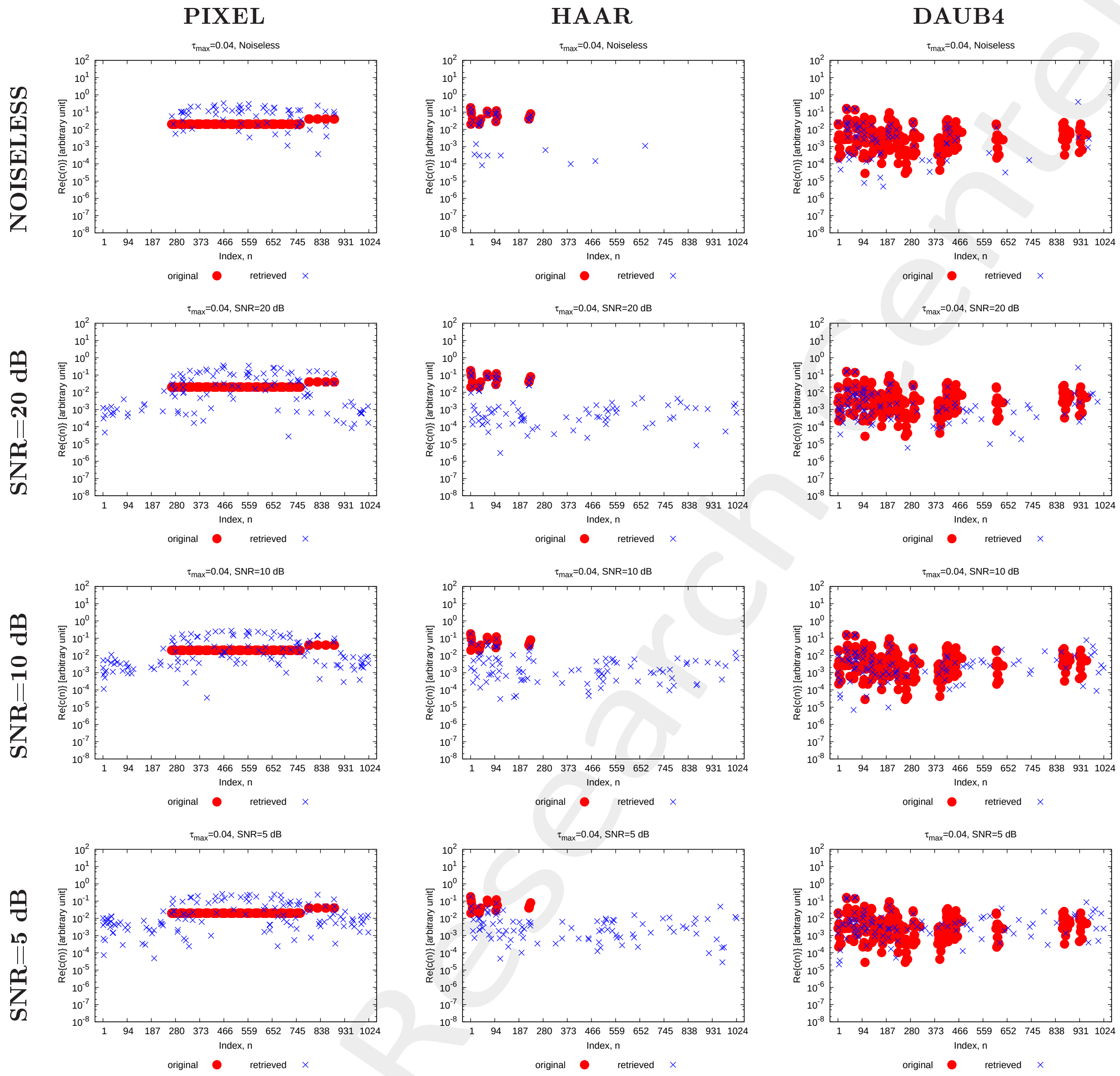

Figure 9: Absolute value (dB) of the actual and retrieved coefficients considering different wavelet expansions.

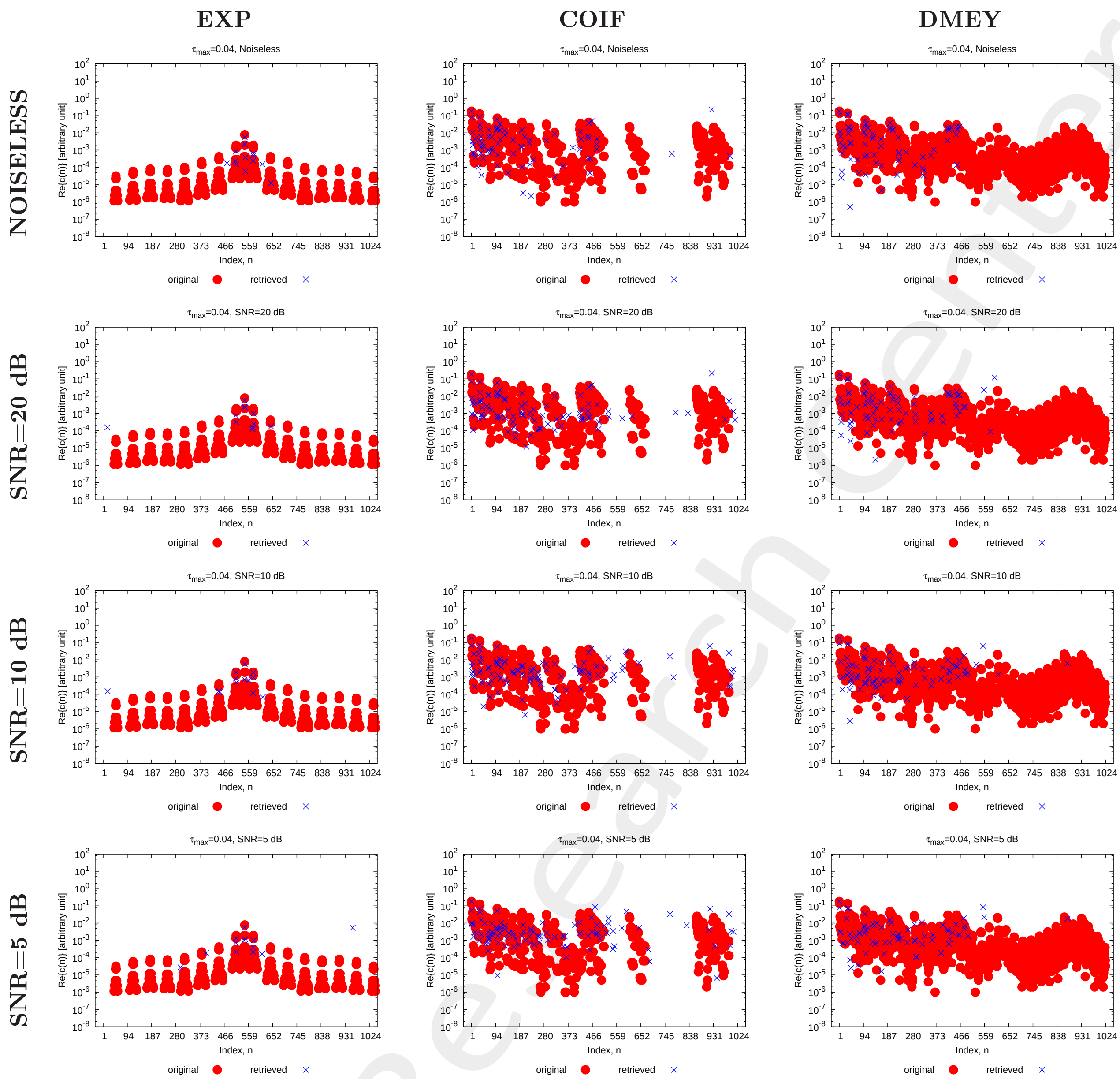

Figure 10: Absolute value (dB) of the actual and retrieved coefficients considering different wavelet expansions.

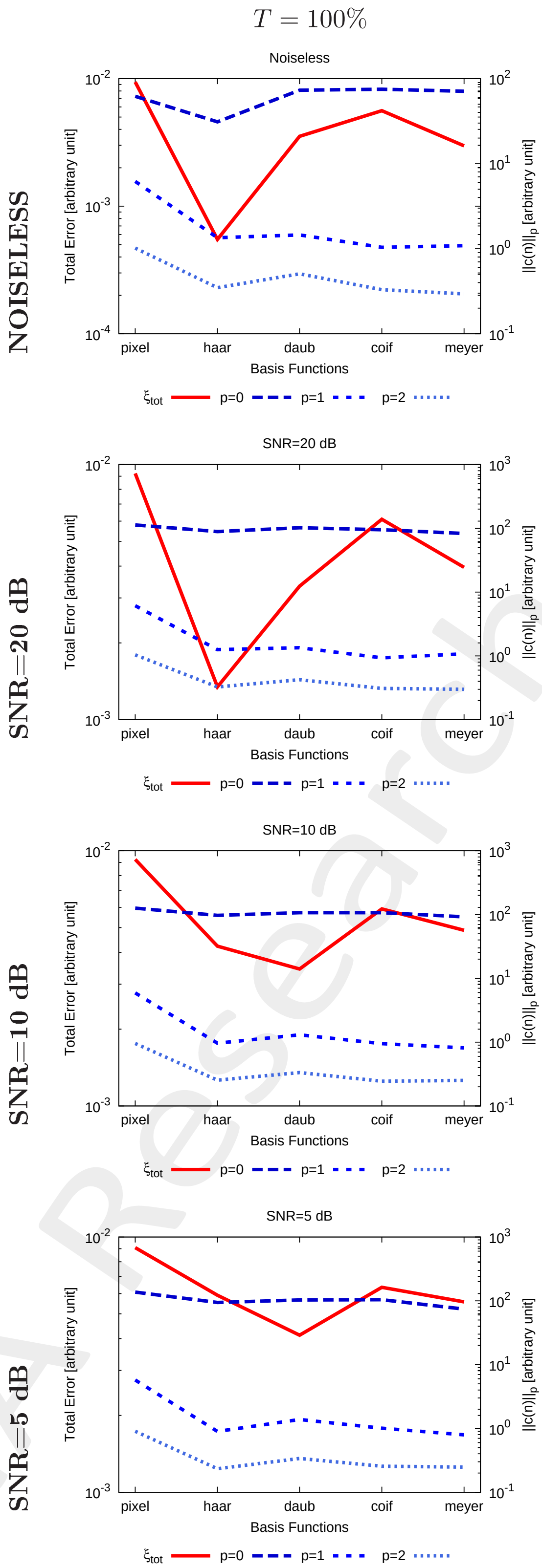

Figure 11: $[T = 100\%]$ - Comparison of ξ_{tot}, and L_0, L_1, L_2 Norms of the retrieved basis expansion coefficients, for each alphabet basis.

	$L_0 - norm$					
SNR [dB]	$Pixel$	$Haar$	$Daub4$	$Coiflet$	$DMeyer$	Exp
$Actual$	272	21	236	459	1024	252
$Noiseless$	62	**31**	73	75	71	14
20	113	89	102	95	**83**	11
10	126	97	107	107	**92**	13
5	137	94	103	104	**74**	13
	$L_1 - norm$					
SNR [dB]	$Pixel$	$Haar$	$Daub4$	$Coiflet$	$DMeyer$	Exp
$Actual$	5.76	1.41	2.39	3.07	3.16	3.1×10^{-2}
$Noiseless$	6.18	1.35	1.45	1.04	1.09	1.4×10^{-2}
20	6.13	1.26	1.34	0.93	1.10	1.3×10^{-2}
10	5.92	0.96	1.30	0.94	0.81	1.4×10^{-2}
5	5.73	0.90	1.38	1.01	0.79	1.7×10^{-2}
	$L_2 - norm$					
SNR [dB]	$Pixel$	$Haar$	$Daub4$	$Coiflet$	$DMeyer$	Exp
$Actual$	0.36	0.36	0.36	0.36	0.36	9.2×10^{-3}
$Noiseless$	1.02	0.35	0.51	0.33	0.29	6.6×10^{-3}
20	1.04	0.34	0.42	0.31	0.30	6.6×10^{-3}
10	0.96	0.25	0.33	0.24	0.25	6.5×10^{-3}
5	0.90	0.23	0.33	1.25	0.24	8.1×10^{-3}

Table 1: $[T = 100\%]$ - Number of the retrieved non-zero coefficients ($L_0 - norm$), $L_1 - norm$, and $L_2 - norm$ using different wavelet functions.

Thresholded Analysis:

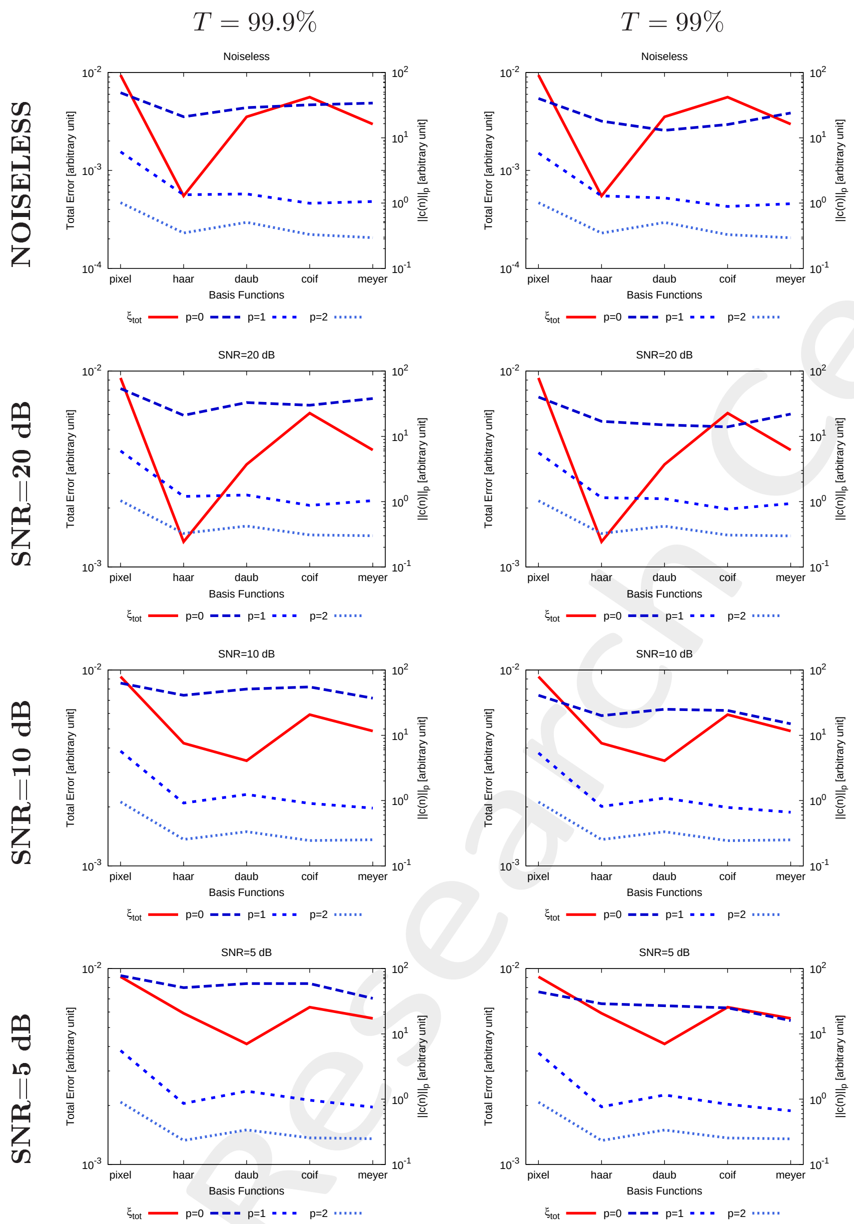

Figure 12: Comparison of ξ_{tot}, and L_0, L_1, L_2 Norms of the retrieved basis expansion coefficients, for each alphabet basis.

	$L_0 - norm$				
SNR [dB]	$Pixel$	$Haar$	$Daub4$	$Coiflet$	$DMeyer$
$Actual$	272	21	236	459	1024
$Noiseless$	49	21	29	32	34
20	54	21	33	30	38
10	63	41	51	55	37
5	78	51	59	59	35
	$L_1 - norm$				
SNR [dB]	$Pixel$	$Haar$	$Daub4$	$Coiflet$	$DMeyer$
$Actual$	5.76	1.41	2.39	3.07	3.16
$Noiseless$	6.10	1.34	1.38	0.99	1.06
20	5.98	1.20	1.26	0.88	1.04
10	5.73	0.92	1.24	0.90	0.77
5	5.55	0.86	1.32	0.96	0.75
	$L_2 - norm$				
SNR [dB]	$Pixel$	$Haar$	$Daub4$	$Coiflet$	$DMeyer$
$Actual$	0.36	0.36	0.36	0.36	0.36
$Noiseless$	1.02	0.35	0.51	0.33	0.29
20	1.04	0.33	0.42	0.31	0.30
10	0.96	0.25	0.33	0.24	0.25
5	0.90	0.23	0.34	0.25	0.25

Table 2: $[T = 99.9\%]$ - Number of the retrieved non-zero coefficients ($L_0 - norm$), $L_1 - norm$, and $L_2 - norm$ using different wavelet functions.

	$L_0 - norm$				
SNR [dB]	$Pixel$	$Haar$	$Daub4$	$Coiflet$	$DMeyer$
$Actual$	272	21	236	459	1024
$Noiseless$	40	18	13	16	24
20	40	17	15	14	22
10	41	20	25	24	15
5	44	29	27	25	16
	$L_1 - norm$				
SNR [dB]	$Pixel$	$Haar$	$Daub4$	$Coiflet$	$DMeyer$
$Actual$	5.76	1.41	2.39	3.07	3.16
$Noiseless$	5.83	1.29	1.20	0.89	0.98
20	5.62	1.15	1.11	0.77	0.93
10	5.36	0.81	1.09	0.79	0.66
5	5.10	0.76	1.16	0.84	0.66
	$L_2 - norm$				
SNR [dB]	$Pixel$	$Haar$	$Daub4$	$Coiflet$	$DMeyer$
$Actual$	0.36	0.36	0.36	0.36	0.36
$Noiseless$	1.01	0.35	0.50	0.33	0.29
20	1.03	0.33	0.42	0.31	0.30
10	0.95	0.25	0.33	0.24	0.25
5	0.90	0.23	0.34	0.25	0.25

Table 3: $[T = 99\%]$ - Number of the retrieved non-zero coefficients ($L_0 - norm$), $L_1 - norm$, and $L_2 - norm$ using different wavelet functions.

Resume:

	$T = 100\%$				
SNR [dB]	$Pixel$	$Haar$	$Daub4$	$Coiflet$	$DMeyer$
$Noiseless$	62	**31**	73	75	71
20	113	89	102	95	**83**
10	126	97	107	107	**92**
5	137	94	103	104	**74**
	$T = 99.9\%$				
SNR [dB]	$Pixel$	$Haar$	$Daub4$	$Coiflet$	$DMeyer$
$Noiseless$	49	**21**	29	32	34
20	54	**21**	33	30	38
10	63	41	51	55	**37**
5	78	51	59	59	**35**
	$T = 99\%$				
SNR [dB]	$Pixel$	$Haar$	$Daub4$	$Coiflet$	$DMeyer$
$Noiseless$	40	18	**13**	16	24
20	40	17	15	**14**	22
10	41	20	25	24	**15**
5	44	29	27	25	**16**

Table 4: $L_0 - norm$.

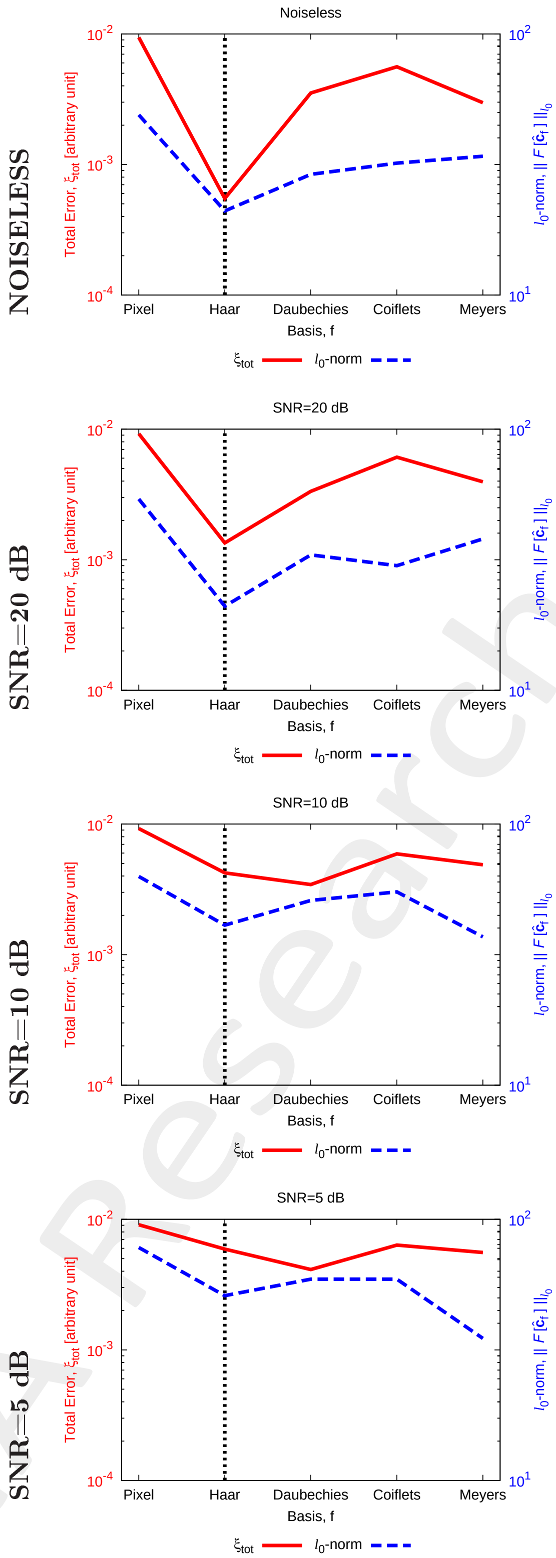

Figure 13: $L_0 - norm$ vs Total Error, considering $T = 99.9\%$.

Comparison SoA:

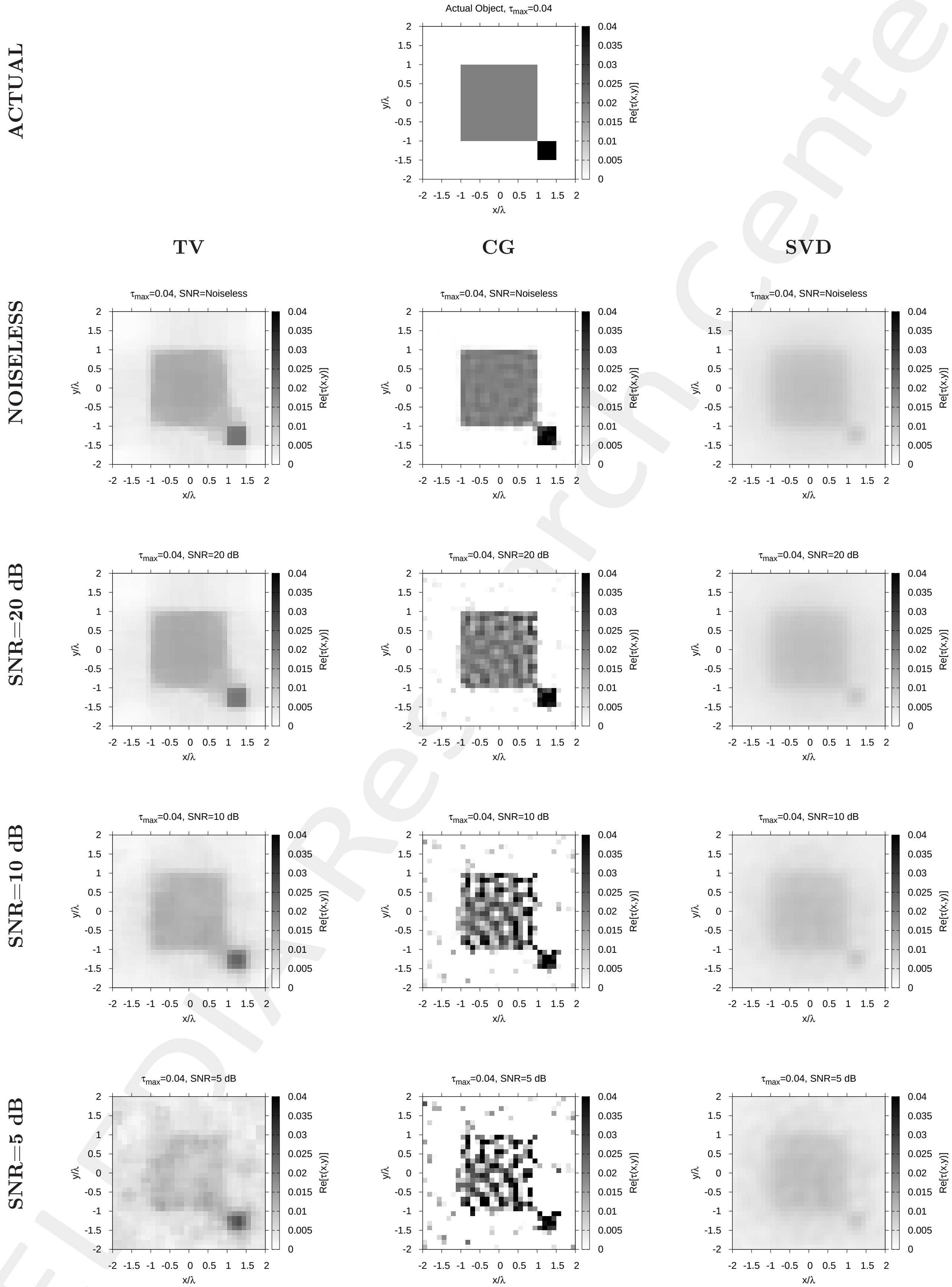

Figure 14: Actual and retrieved object considering different wavelet expansions.

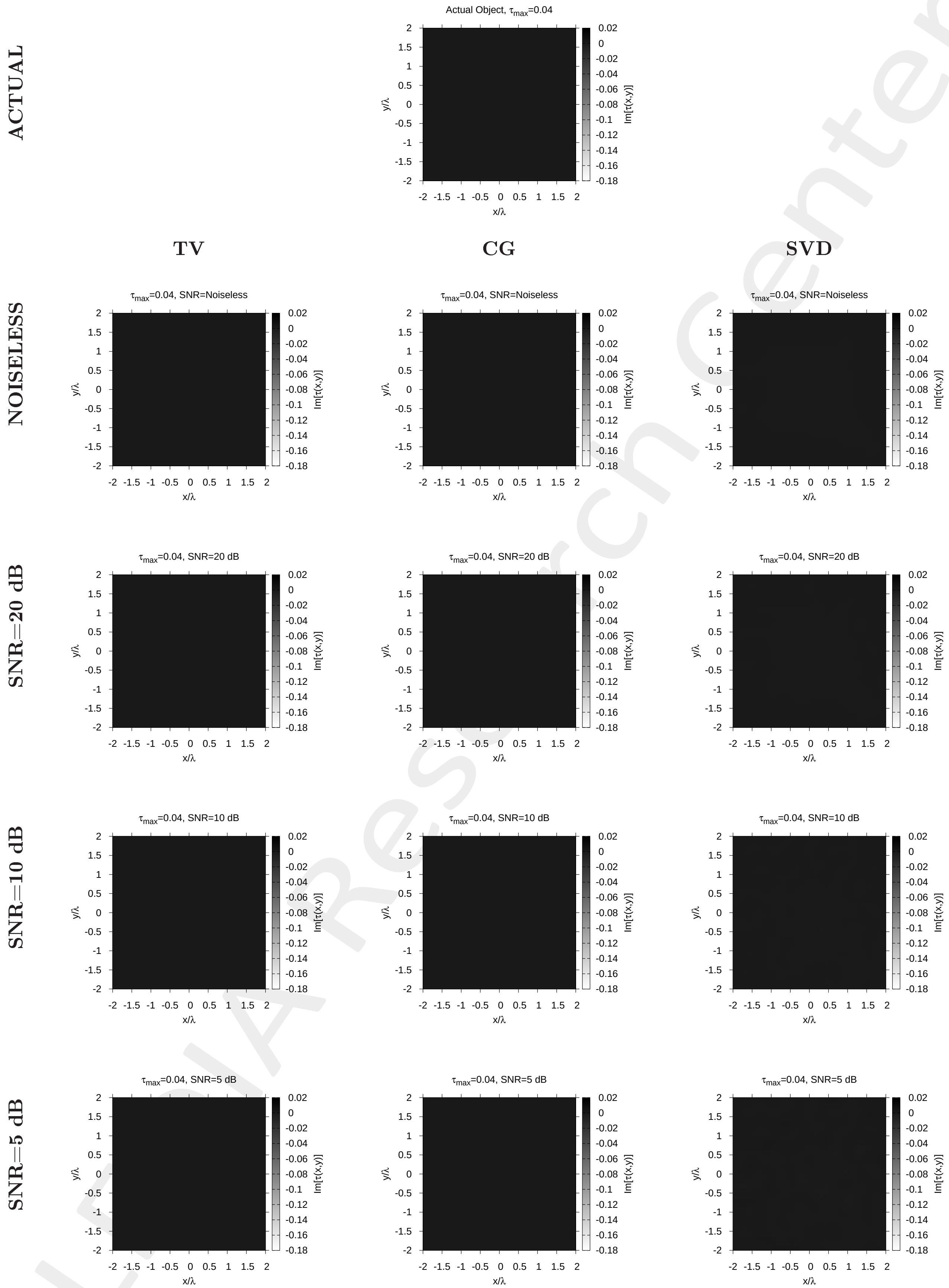

Figure 15: Actual and retrieved object considering different wavelet expansions.

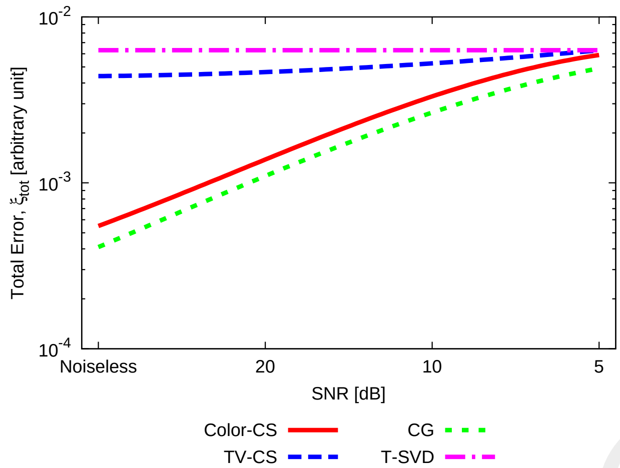

Figure 16: Comparison with SoA - Total Error vs SNR, considering $T = 99.9\%$.

SNR [dB]	**TV [s]**	**CG [s]**	**SVD [s]**	**ALPHABET [s]**
Noiseless	3.8×10^2	6.9×10^3	4.3×10^1	1.0×10^3
20	3.8×10^2	6.1×10^3	3.5×10^1	9.6×10^2
10	3.8×10^2	5.4×10^3	3.6×10^1	9.3×10^2
5	3.9×10^2	5.6×10^3	3.5×10^1	$7.9. \times 10^2$

Table 5: Timings.

References

[1] A. Massa, P. Rocca, and G. Oliveri, “Compressive sensing in electromagnetics - A review,” *IEEE Antennas Propag. Mag.*, pp. 224-238, vol. 57, no. 1, Feb. 2015.

[2] A. Massa and F. Texeira, Guest-Editorial: Special Cluster on Compressive Sensing as Applied to Electromagnetics, *IEEE Antennas Wireless Propag. Lett.*, vol. 14, pp. 1022-1026, 2015.

[3] G. Oliveri, N. Anselmi, and A. Massa, “Compressive sensing imaging of non-sparse 2D scatterers by a total-variation approach within the Born approximation,” *IEEE Trans. Antennas Propag.*, vol. 62, no. 10, pp. 5157-5170, Oct. 2014.

[4] L. Poli, G. Oliveri, and A. Massa, “Imaging sparse metallic cylinders through a Local Shape Function Bayesian Compressive Sensing approach,” *J. Opt. Soc. Am. A*, vol. 30, no. 6, pp. 1261-1272, 2013.

[5] F. Viani, L. Poli, G. Oliveri, F. Robol, and A. Massa, “Sparse scatterers imaging through approximated multitask compressive sensing strategies,” *Microwave Opt. Technol. Lett.*, vol. 55, no. 7, pp. 1553-1558, Jul. 2013.

[6] M. Salucci, G. Oliveri, and A. Massa, “GPR prospecting through an inverse scattering frequency-hopping multi-focusing approach,” *IEEE Trans. Geosci. Remote Sens.*, vol. 53, no. 12, pp. 6573-6592, Dec. 2015.

[7] M. Salucci, L. Poli, N. Anselmi and A. Massa, “Multifrequency particle swarm optimization for enhanced multiresolution GPR microwave imaging,” *IEEE Trans. Geosci. Remote Sens.*, vol. 55, no. 3, pp. 1305-1317, Mar. 2017.

[8] M. Salucci, L. Poli, and A. Massa, “Advanced multi-frequency GPR data processing for non-linear deterministic imaging,” Signal Processing - Special Issue on ’Advanced Ground-Penetrating Radar Signal-Processing Techniques,’ vol. 132, pp. 306-318, March 2017.

[9] L. Poli, G. Oliveri, P. Rocca, and A. Massa, “Bayesian compressive sensing approaches for the reconstruction of two-dimensional sparse scatterers under TE illumination,” *IEEE Trans. Geosci. Remote Sens.*, vol. 51, no. 5, pp. 2920-2936, May 2013.

[10] L. Poli, G. Oliveri, and A. Massa, “Microwave imaging within the first-order Born approximation by means of the contrast-field Bayesian compressive sensing,” *IEEE Trans. Antennas Propag.*, vol. 60, no. 6, pp. 2865-2879, Jun. 2012.

[11] G. Oliveri, P. Rocca, and A. Massa, “A bayesian compressive sampling-based inversion for imaging sparse scatterers,” *IEEE Trans. Geosci. Remote Sens.*, vol. 49, no. 10, pp. 3993-4006, Oct. 2011.

[12] G. Oliveri, L. Poli, P. Rocca, and A. Massa, “Bayesian compressive optical imaging within the Rytov approximation,” *Optics Letters*, vol. 37, no. 10, pp. 1760-1762, 2012.

[13] L. Poli, G. Oliveri, F. Viani, and A. Massa, "MT-BCS-based microwave imaging approach through minimum-norm current expansion," *IEEE Trans. Antennas Propag.*, vol. 61, no. 9, pp. 4722-4732, Sep. 2013.

[14] N. Anselmi, G. Oliveri, M. Salucci, and A. Massa, "Wavelet-based compressive imaging of sparse targets" *IEEE Trans. Antennas Propag.*, vol. 63, no. 11, pp. 4889-4900, Nov. 2015.

[15] N. Anselmi, G. Oliveri, M. A. Hannan, M. Salucci, and A. Massa, "Color compressive sensing imaging of arbitrary-shaped scatterers," *IEEE Trans. Microw. Theory Techn.*, vol. 65, no. 6, pp. 1986-1999, Jun. 2017.

[16] F. Viani, G. Oliveri, and A. Massa, "Compressive sensing pattern matching techniques for synthesizing planar sparse arrays," *IEEE Trans. Antennas Propag.*, vol. 61, no. 9, pp. 4577-4587, Sept. 2013.

[17] G. Oliveri, M. Salucci, and A. Massa, "Synthesis of modular contiguously clustered linear arrays through a sparseness-regularized solver," *IEEE Trans. Antennas Propag.*, vol. 64, no. 10, pp. 4277-4287, Oct. 2016.

[18] P. Rocca, M. A. Hannan, M. Salucci, and A. Massa, "Single-snapshot DoA estimation in array antennas with mutual coupling through a multi-scaling BCS strategy," *IEEE Trans. Antennas Propag.*, vol. 65, no. 6, pp. 3203-3213, Jun. 2017.

[19] P. Rocca, M. Benedetti, M. Donelli, D. Franceschini, and A. Massa, "Evolutionary optimization as applied to inverse problems," *Inverse Probl.*, vol. 25, pp. 1-41, Dec. 2009.

[20] P. Rocca, G. Oliveri, and A. Massa, "Differential Evolution as applied to electromagnetics," *IEEE Antennas Propag. Mag.*, vol. 53, no. 1, pp. 38-49, Feb. 2011.